

# The Analysis of Isochrone Fitting Methods for Red Giant Branch Photometry, and Tip Red Giant Branch Distance Determination

C. M. Frayn<sup>1</sup>, G. F. Gilmore<sup>1</sup>

<sup>1</sup> *Institute of Astronomy, University of Cambridge, Cambridge, CB3 0HA, UK*

Submitted to MNRAS, September 2002

## ABSTRACT

We consider the procedure of isochrone fitting and its application to the study of red giant branch (RGB) photometry in old stellar populations. This is extended to consider the problems introduced by the inclusion of lower-magnitude regions of the Colour Magnitude Diagram (CMD). We refer especially to our previous paper Frayn & Gilmore (2002), where the details of our isochrone interpolation and fitting code are explained.

We address the systematic errors inherent in the process of isochrone fitting, and investigate the extent to which simple stellar populations can be recovered from noisy photometric data. We investigate the effects caused by inaccurate distance estimates, isochrone model variation and photometric errors. We present results from two studies of approximately coeval stellar populations, those of the Milky Way Globular Cluster System (MWGCS), and the Ursa Minor dwarf spheroidal galaxy.

In addition, we introduce a new method for estimating distances using photometry of the tip of the RGB which is significantly more robust than the standard edge-detection filter.

**Key words:** galaxies: haloes – stars: Population II – methods: data analysis – Hertzsprung-Russell (HR) diagram – galaxies: distances and redshifts – stars: distances

## 1 INTRODUCTION

In our first paper, Frayn & Gilmore 2002 (henceforth FG1), we introduced isochrone-fitting methods to analyse photometric data on red-giant branch populations in the haloes of nearby galaxies. Best-fitting metallicity distributions were obtained by generating a probability matrix mapping each star in a theoretical or experimental Colour-Magnitude Diagram onto an occupation probability for each isochrone in the input model set. Isochrone weighting coefficients were then optimised to produce a profile which maximised the likelihood of producing the observed CMD under a set of constraints. Most importantly, we considered only a high-age coeval distribution, thus largely overcoming the problems of the age-metallicity degeneracy. We refer the reader to FG1 for more details.

In FG1, we treated many sources of error in an attempt to gain the most accurate metallicity distribution possible. However, it is clear that the technique of isochrone fitting is extremely problematic, and many effects need careful consideration if incorrect or overly optimistic conclusions are to be avoided.

In this paper, we re-examine the most important sources of systematic error, and investigate the effects that errors have on the conclusions we can draw from RGB studies. We also consider the effects of including deeper photometry down to the Horizontal Branch (HB) or Main-Sequence Turn-Off (MSTO) regions, and compare the results gained from analysis of the entire CMD to those gained from considering the RGB only.

In order of importance, we investigate the primary causes of error that we have discovered, concentrating on the methods outlined in FG1. We identify the errors inherent in those, and indeed any similar methods, in a quantitative manner. As an appendix, we consider the uncertainties inherent in the isochrones themselves.

We also present a new method for obtaining distance estimates from RGB photometry that yields more accurate results than a traditional edge detection implementation for the majority of cases, and is robust even to severe photometric errors.

## 2 LIMITATIONS DUE TO THE ANALYSIS METHOD

In this section, we deal with the problems caused by the fundamental assumptions that we have to put into our population analysis, and investigate the degree to which we can resolve these problems using different methods.

### 2.1 Age-metallicity degeneracy

This is the main problem that must be faced in the analysis of RGB stellar populations. As is well known, and reviewed in FG1, the effects of increasing metal abundance on stellar isochrones are remarkably similar to those of increasing age. In fact, with the absence of any other diagnostic methods, it becomes impossible to separate the two effects in some parts of the CMD. This effect is particularly bad in the RGB which has no sharp features to help distinguish between the contrasting effects.

We avoid this problem by assuming a high age, and then reducing the data as if it were coeval. This method is justified when dealing with primarily old populations where the effects of age on the RGB become significantly lessened (see FG1). However, metallicity still has noticeable effects, and therefore we can get a rough metal abundance distribution without having to worry too much about the age spread.

Here we test this hypothesis, investigating the degree to which the coeval assumption in old RGB populations holds true. We analyse synthetic CMDs generated by our own code, and using the coeval fitting routines outlined in FG1. First of all we consider the pristine CMD, that is without any photometric or Poisson errors added into the dataset. We then reduce it with only a tiny photometric error, essentially recovering the degree to which the theoretical isochrones overlap. This tells us something fundamental about the actual limits to which we can trust isochrone fitting, regardless of the data quality. Fig. 1 shows the results of this test.

The expectation is that we can only ever hope to achieve this quality of data reduction at best on a true data set, simply because of the photometric errors involved. However, when attempting to recover a very narrow distribution we may appear to manage slightly better. This is simply because, once accurate errors are considered, our maximum likelihood method will attempt to narrow the metallicity distributions it finds if there is insufficient data to suggest a substantial spread. In the absence of any prior information to the contrary it is safe to assume that the stellar populations are relatively simple. In general, stars don't vary smoothly in metallicity as a function of mass, which would be the effect caused by an incorrect age assumption.

If one repeats the above experiment, but this time includes the full Poisson errors in both the creation of the CMD and its analysis, and one also incorporates fixed photometric errors, in this case we used 3%, then the reduction proceeds rather more smoothly. The code has insufficient evidence to suggest that the populations are anything other than delta-function in metallicity, and assumes that the remainder of the spread is due to photometric and Poisson errors. Hence the resulting metallicity distribution is significantly better.

These results are shown in Fig. 2. In this case we con-

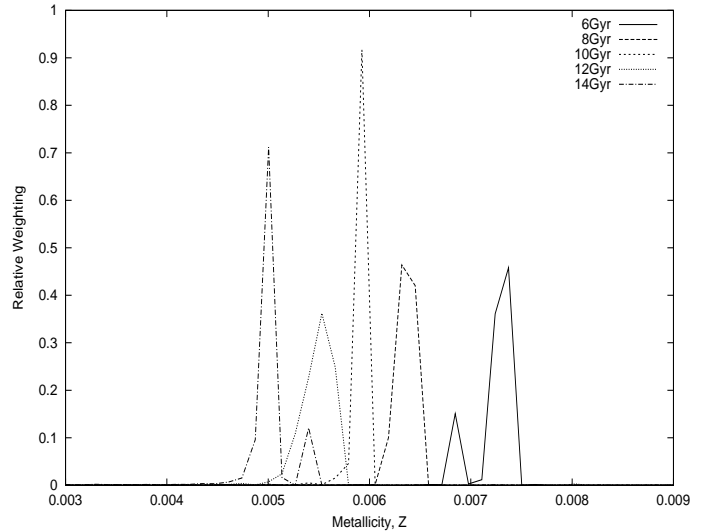


**Figure 1.** A single delta-function RGB population at a metallicity of  $Z = 0.006$  and age 10 Gyr. This was then reduced assuming incorrect ages between 6 Gyr and 14 Gyr, i.e.  $\pm 40\%$ . Although the error is noticeable, it is not drastic, even at a large age error. Note the shortened x-axis scale.

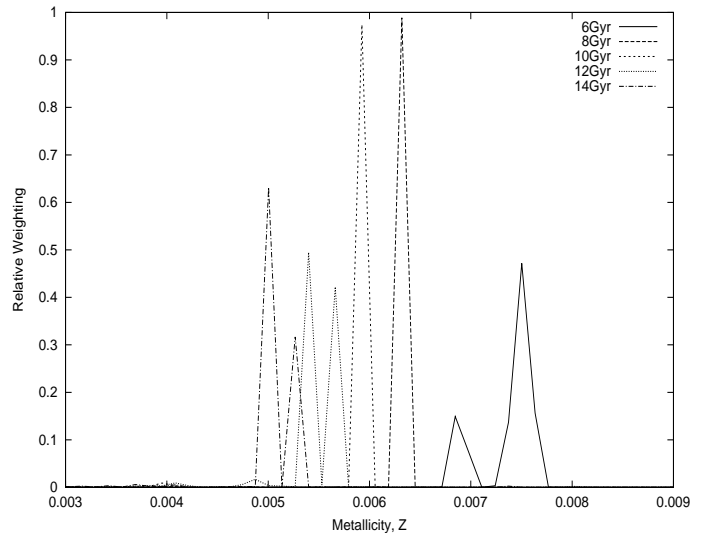


**Figure 2.** A single delta-function population at a metallicity of  $Z = 0.006$  and age 10 Gyr. The photometry was complete to beneath the MSTO. This was then reduced assuming incorrect ages between 6 Gyr and 14 Gyr, i.e.  $\pm 40\%$ . We introduced accurate photometric and Poisson errors into the artificial datasets, and used the same values for our data analysis. Using accurate photometric errors helps in retrieving a more accurate guess to an input metallicity distribution.

sider photometry complete to the MSTO to demonstrate that even problems fitting the HB are lessened once proper errors are considered. This is an important result – HB contamination causes problems even when dealing primarily with RGB photometry, if the completeness limit is deeper than the top few magnitudes of the RGB.

Because of this inherent problem with our methods, we will encounter problems with populations which are not truly of one unique metallicity, but instead have some in-

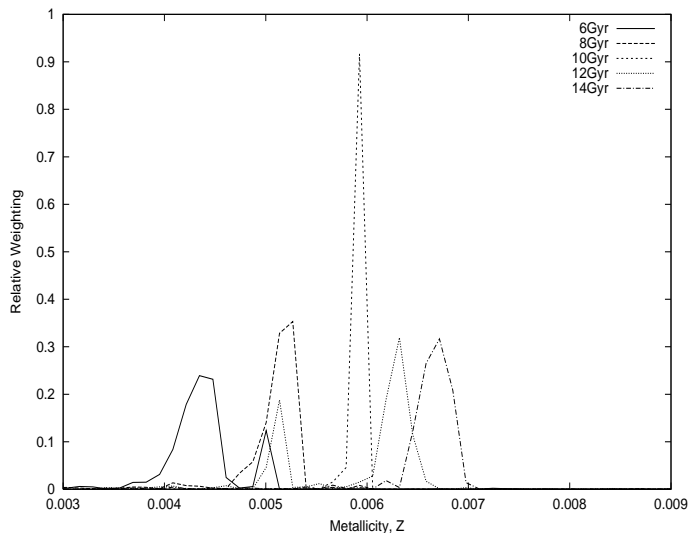


**Figure 3.** A set of delta-function RGB populations at a metallicity of  $Z = 0.006$ , but ages varying between 6 Gyr and 14 Gyr. All were reduced under the assumed age of 10 Gyr. Errors are less severe for older populations.

herent spread in metallicity which should be recovered. Often this spread is reduced due to the likelihood optimisation methods employed. However, the perpendicular distance method (see FG1) seems to recover input metallicity spread far more efficiently than a Gaussian method. In addition, underestimating the errors helps recover the spread, albeit at a slight penalty in removing experimental noise.

### 2.1.1 Introducing age errors

Next we tested the reduction of populations generated at differing ages, with an assumed age of 10 Gyr. These results are shown in Fig. 3. Once again, the general form of the population is recovered, though this recovery is obviously worse in the case of the younger populations.

In all the cases investigated, the error becomes much greater when one ventures to lower ages rather than high ages. The difference between populations of 10 Gyr and 14 Gyr is not too great, but the difference in shape between 10 Gyr and 6 Gyr, though the same  $\Delta age$ , is far greater. At 6 Gyr, the isochrones include the effect of intermediate-age Asymptotic Giant Branch (AGB) stars, and the change in isochrone slope becomes greater per unit age interval. Isochrone evolution is a roughly logarithmic process, and most isochrone sets are logarithmically spaced in age to account for this.

## 2.2 Distance degeneracy

One further degeneracy problem must be considered in order to understand fully the errors inherent in such a technique. That is the principle of metallicity-distance degeneracies.

So far we have considered populations located at an accurately-known location. We have considered that the distance modulus of the target population is known precisely. In fact, this is rarely the case. For distant targets, the distance might be unknown by a large percentage. At the Virgo

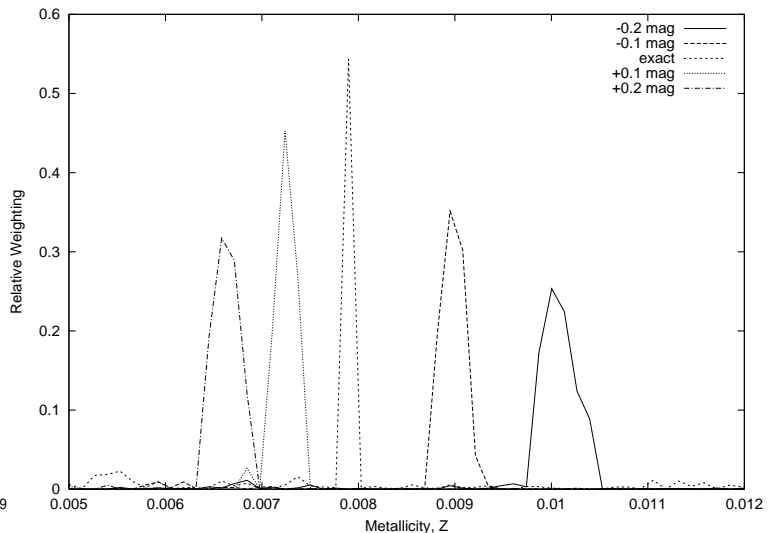


**Figure 4.** A single delta-function population at a metallicity of  $Z = 0.008$ . This was then reduced assuming slight errors in the distance modulus varying between  $-0.2$  and  $+0.2$ .

cluster, the best guess distances to target galaxies are known only to around the  $\pm 0.2$  magnitude level (e.g. Ferrarese et al. (1996)) from Cepheid variable methods. It is important to measure the extent of the problems caused by assuming an incorrect distance modulus for a target population.

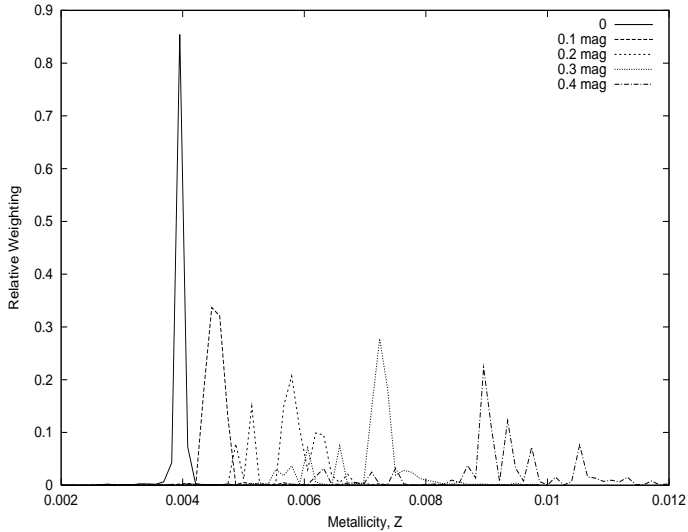
In order to test this, we have generated an artificial CMD as described in our previous paper. We have generated a single delta-function population at the distance of 16 Mpc, consisting of 10,000 stars. We then reduced this population using our numerical techniques assuming the true distance modulus of  $+31 mag$ , and then over- and under-estimating this value by  $0.1 mag$  and  $0.2 mag$ . We considered only the RGB for analysis, as before, using the 48 RGB stars thus obtained.

Fig. 4 shows the results of this test. An error of just  $\pm 0.2$  magnitudes in the estimated distance modulus can actually cause appreciable problems with the recovered metallicity spread. However, we can account for this problem in our analysis of the recovered metal abundance distributions. Several methods can be used to estimate distances to nearby galaxies, including Cepheid variable studies, and Tip-Red Giant Branch (TRGB) photometry.

A distance overestimate of  $+0.2 mag$  equates to an underestimate of the true metallicity by approximately 20%. Underestimating the distance by the same amount equates to an overestimate of the true metallicity by 25%. Both error directions also cause a spread in the recovered metallicity distribution. Even a 25% error in the recovered metal abundance is not an enormous problem when considering the difference between an early, low metallicity population and a late, high metallicity population whose metal abundances might well vary by a factor of three or more.

## 2.3 Reddening effects

Interstellar reddening affects the accuracy to which we can understand any stellar population. In the optical regime, dust causes a wavelength-dependent absorption feature



**Figure 5.** A single delta-function population at a metallicity of  $Z = 0.004$  and age 10 Gyr which has been reddened by varying amounts, and then reduced assuming no reddening whatsoever. Reddening causes an overestimate of the true central metallicity value and a spread in the distribution. The five plots represent no reddening, and then for  $V$ -band extinction of between 0.1 and 0.4 mags. The effect on  $V - I$  colours was taken from Mathis (1990).

which decreases apparent luminosities more strongly in the blue end of the spectrum than in the red. Hence, the  $V$  and  $I$  luminosities are reduced, but to differing amounts, therefore also altering the  $V - I$  colours correspondingly.

To test the actual effect of reddening on a simple stellar population, we have run a series of simulations. We applied varying levels of reddening to a simple stellar population, and ran this through our code assuming no reddening whatsoever. The results are shown in Fig. 5. We assume the extinction model proposed by Mathis (1990).

Reddening causes two effects. Firstly, it dims the stars in each optical filter, simulating effects similar to a distance increase. Secondly, it shifts the colours of the stars redward, thereby mimicking a slight metallicity increase.

### 3 TRGB DISTANCE ESTIMATION

We have shown that the assumed distance for a stellar population can indeed cause several problems if it is significantly different to the true value. It makes sense therefore to use our RGB photometry in order to estimate a good fit to the distance modulus using the TRGB distance estimation technique, outlined by Salaris & Cassisi (1997) amongst others.

This method relies on the fact that the total bolometric magnitude of the tip of the RGB appears to be approximately constant, regardless of age and metallicity, for stable old populations. The absolute  $I$  magnitude of the tip is also approximately constant, at a value of  $I \simeq -4.05$  mag, varying by no more than 0.1 magnitude for  $-2.2 < [Fe/H] < -0.7$ , according to Da Costa & Armandroff (1990).

We can use this method therefore to check the assumed distance modulus and to verify that a sensible value has been used. To do this, we require an edge fitting method

which will allow us to detect the apparent  $I$  magnitude of the TRGB from our data.

There is some discrepancy in the literature about the true position of the ‘edge’ in this situation. Many people follow the method of Sakai et al. (1996), henceforth S96, who use a discrete Sobel edge detection filter to find the assumed tip. We remain sceptical about this particular method as it is easily swamped by experimental Poisson statistics, especially in the low-number count regime.

We tentatively adopt the Sobel edge-detection method in order to test the method. Taking the given distance modulus as a first guess, we generated a binned histogram between  $\pm 1$  mag of this value using an adaptive binning technique which ensures that the number counts in each bin remain above a certain low threshold.

An example of the theory behind this method is illustrated in figure 6. Here we have generated a large artificial population using the methods outlined in FG1, with a simple age and metallicity profile and no photometric errors. We present a binned  $I$ -magnitude luminosity function for one magnitude either side of the expected RGB tip. An ‘edge’ is clearly seen.

Here we use the value of  $I_{TRGB} = -4.05$  (Da Costa & Armandroff 1990). Values close to this seem to be preferred by most studies. See e.g. Salaris, Cassisi & Weiss (2002). Most authors seem to derive values slightly brighter than  $I_{TRGB} = -4.0$ , though there is a spread of around 0.2 magnitudes in the literature. We acknowledge that Girardi et al. (2000) predict  $I_{TRGB} \simeq -3.95$  from the theoretical isochrone models used in this paper, which agrees slightly better with the position of the edge determined in figure 6. Further work in this paper considers only relative displacement so inaccuracies in this value are not important.

In more realistic stellar populations, there are two additional spreads in the  $I$ -luminosity function. One is the intrinsic spread due to the fact that not all of the stars are of the same metallicity, age and mass, in general. However, there is also an extra spread caused by measurement errors which makes this edge-detection method extremely difficult to apply. Even without measurement errors, one would not expect such a distinct edge as that seen in Fig. 6 in most populations, simply because they are not coeval. We consider an alternative : to calibrate the TRGB distances using an appropriate Gaussian cutoff, and then search for the mean. This is much less susceptible to experimental errors and gives an obvious target to identify.

First, we bin the data as above. Then we fit a Gaussian cutoff to the luminosity function of the form;

$$\begin{aligned} \Phi &= Ae^{\frac{-(m_I - b)^2}{2c^2}} + d \quad \text{for } m_I > b \\ \Phi &= A + d \quad \text{otherwise} \end{aligned} \quad (1)$$

and solve for the best-fitting values for the four parameters.  $A$  gives a scaling value,  $b$  gives an  $I$ -magnitude shift,  $c$  gives a scale length for the TRGB tail, and  $d$  gives a constant background offset.

Once these four parameters have been found, then we require the  $I$ -magnitude of the maximal gradient in the luminosity function, or alternatively, the point where the second derivative is zero. Analytically, this is at the value  $I = c + b$ , which can then be calculated from the fit parameters. This gives us a good estimate for the TRGB magnitude,

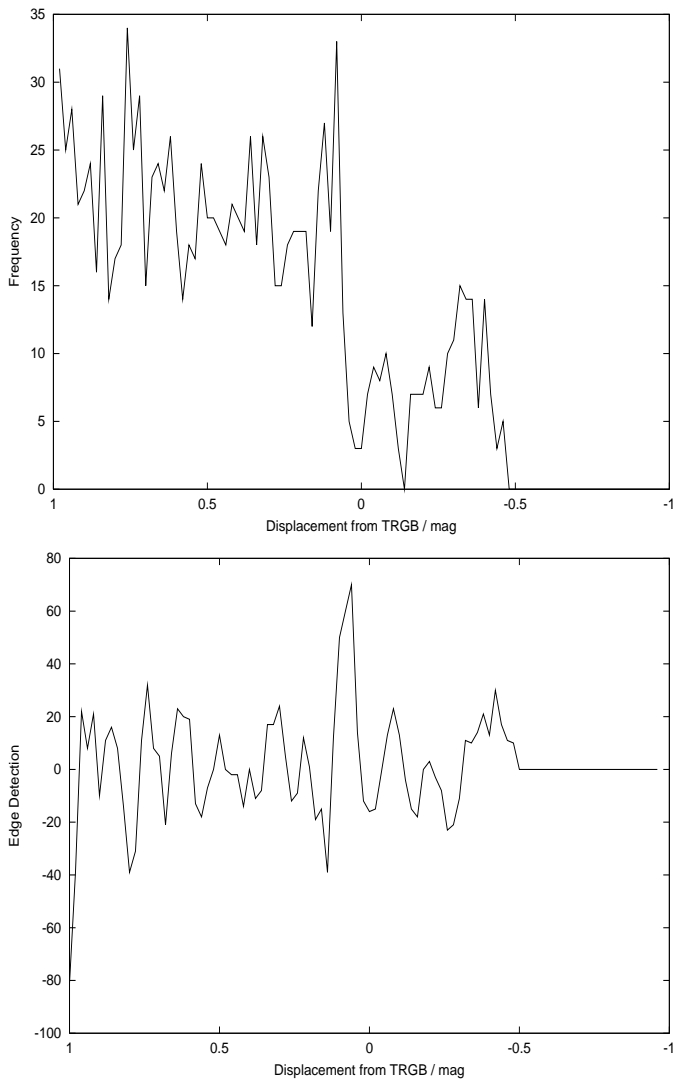


**Figure 6.** An  $I$ -magnitude luminosity function for a coeval artificial population at an age of 10Gyr with a central metallicity of one third solar and an 8% Gaussian spread. No errors of any kind have been added to the dataset, showing far more clearly the location of the TRGB edge. Here, displacement is measured in magnitudes from the theoretical value, uncorrected for metallicity, of  $I = -4.05$  (Da Costa & Armandroff 1990). In the second figure we present the results of a Sobel filter applied to this TRGB luminosity function. A clear edge is detected at a deviation of 0.06 magnitudes beneath the mean experimental value.

which can be compared with the value taken from calibration on nearby globular clusters with well-known distances. Clearly, we could choose any such point on the Gaussian curve and calibrate our relation with comparison to theoretical datasets, but this seems the easiest to define.

In order to compare the two contrasting methods, a set of 16 large CMDs was produced using our code. Each of these was then analysed using both the traditional Sobel edge detection method, and also by fitting a Gaussian cut-off of the form shown above in equation 1. For each dataset we used exactly the same initial conditions, that is a single population with an age of  $10 \pm 0.2 \text{ Gyr}$  and a metallicity of  $Z = 0.006 \pm 0.0005$ . A Salpeter IMF was used, and the Gi-

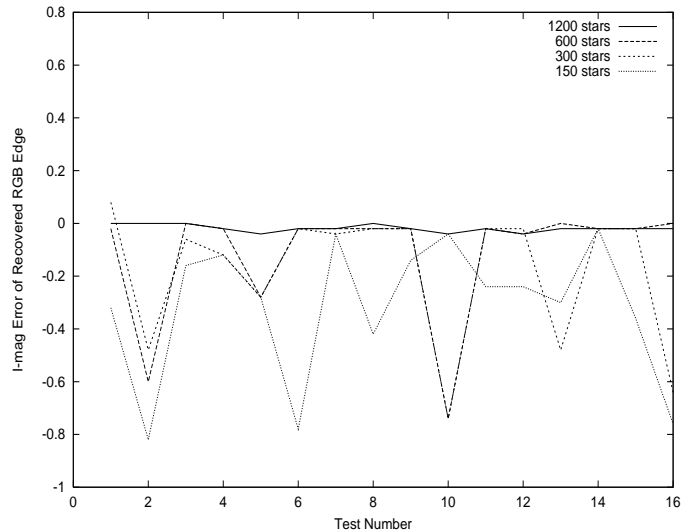


**Figure 7.** Error ( $I_{true} - I_{detected}$ ) on the RGB tip determination using a Sobel filter method like that proposed by S96. The population is a simple stellar cluster at  $10 \pm 0.2 \text{ Gyr}$  and  $Z = 0.006 \pm 0.0005$ . IMF is Salpeter, and photometric errors of 6% were added. 16 test populations were used. Positive values represent an overestimate of the TRGB magnitude.

rardi isochrone set. Realistic photometric errors of 6% were added.

In each set the initial TRGB detection was approximately 1200 stars within one magnitude of the expected TRGB luminosity in  $I$ . Next, half of the stars were removed at random in three steps, thereby creating three further datasets with 600, 300 and 150 stars within one magnitude of the TRGB in each respectively. The same statistical process was repeated on each dataset. Then we repeated the TRGB detection with each dataset after reduction. The results are plotted in figures 7 and 8 for the edge-detection and Gaussian cutoff methods respectively.

What is clear is that the scatter on the values for a Sobel edge fit is smaller for the initial dataset, with approximately 1200 stars within one magnitude of the TRGB. However, as soon as the number of detections reduces significantly beneath 1,000, the Gaussian method produces more reliable results. The one caveat is that, by the nature of the method, the Gaussian technique occasionally produces wildly inaccurate results. This is always easy to detect as the fit Chi-squared value will be very poor, and the values for the parameters  $A, b, c$  and  $d$  will lie outside realistic ranges. For the Sobel method, it is impossible to tell *a posteriori* which results are inaccurate.

Removing those results with clearly poor fits, the average statistical deviation from the true TRGB edge value was calculated in each case of 1,200, 600, 300 and 150 stars within one magnitude of the TRGB. We measured absolute displacement from the mean location of the edge obtained from the largest populations, thus automatically calibrating the Gaussian method and avoiding any problems with the precise magnitude of the TRGB edge used for the Sobel method. For the Sobel filter method, the values were  $\sigma = 0.02, 0.25, 0.31, 0.40$  magnitudes respectively. This means that even with 150 stars within one magnitude of the

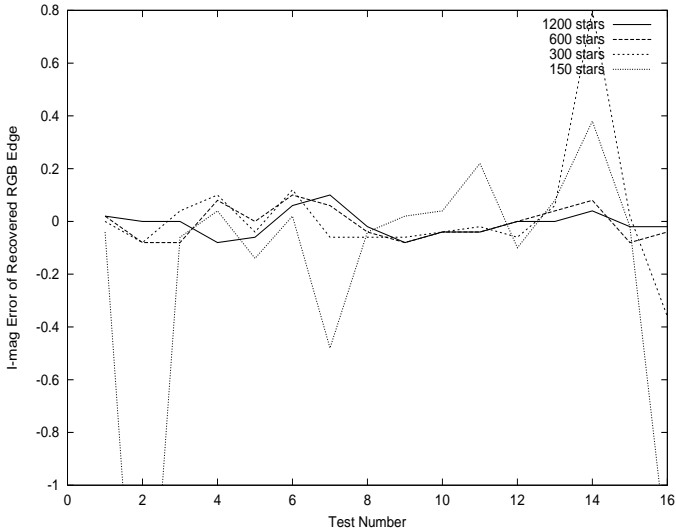


**Figure 8.** Error ( $I_{true} - I_{detected}$ ) on the RGB tip determination using a Gaussian fitting method as described in this section, for the same population described in figure 7. Errors are much smaller in general, except for the occasional large discrepancy caused by a bad fit - a feature that is very easy to test for and avoid. Positive values represent an overestimate of the TRGB magnitude.

TRGB, the expected error on the TRGB detection is 0.4 magnitudes, and could well be much worse.

For the Gaussian method, these values were  $\sigma = 0.05, 0.06, 0.06, 0.14$  magnitudes - an improvement of a factor of almost three on the worst case.

For most datasets we do not expect a substantial number of stars near the TRGB magnitude. Certainly we expect numbers in the low hundreds at best. An example is shown in Fig. 9, showing the TRGB luminosity function for stars in the Ursa Minor dataset analysed in section 5. Clearly, any edge detection on data with such low-number statistics will be largely random. However, by fitting the TRGB with our Gaussian model, as described in this section, we obtain a distance estimate which is only different from the theoretical value of  $(m - M) = 19.11$  (Mateo, 1998) by +0.04 magnitudes. We note that the theoretical value was based on studies of variable stars, so this acts as an independent justification for our techniques.

### 3.1 Varying photometric errors

In order to test this method further, we created a set of datasets identical to those above, but with varying photometric errors between 0% and 10%. These datasets were reduced using the Sobel filter method and the Gaussian method. The population was created so that approximately 500 stars were found within one magnitude of the TRGB in the each dataset, which is more than could be obtained for most observational datasets. The performance of the Sobel method in this test is therefore slightly *better* than might be expected in general. Four populations were created for each photometric error value, and the standard deviation in the errors from the true TRGB location was calculated for each method. The results are shown in Fig. 10.

As the results clearly show, the Gaussian method remains preferable over the Sobel filter method at all photo-

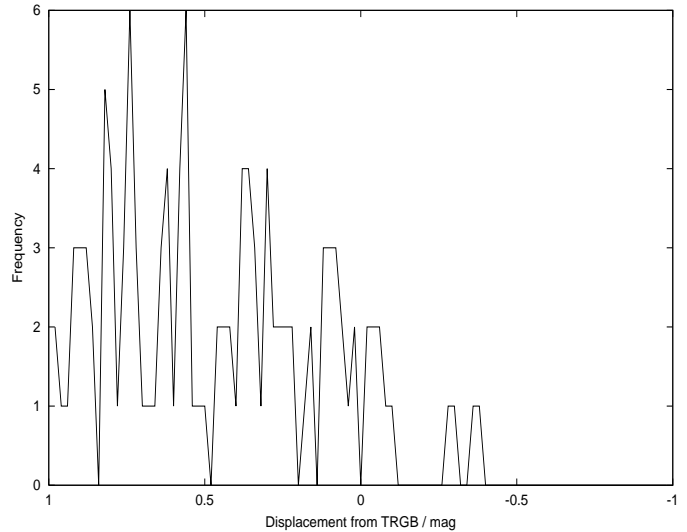


**Figure 9.** The TRGB luminosity function for the Ursa Minor dSph, showing a binned histogram for the 121 stars within one magnitude of the theoretical TRGB. Clearly low-number statistics would make any distance determination using a discrete Sobel filter completely meaningless. Fitting a Gaussian to the results however, as described in this work, gives a distance estimate different from the theoretical value (Mateo, 1998) by just 0.04 magnitudes.

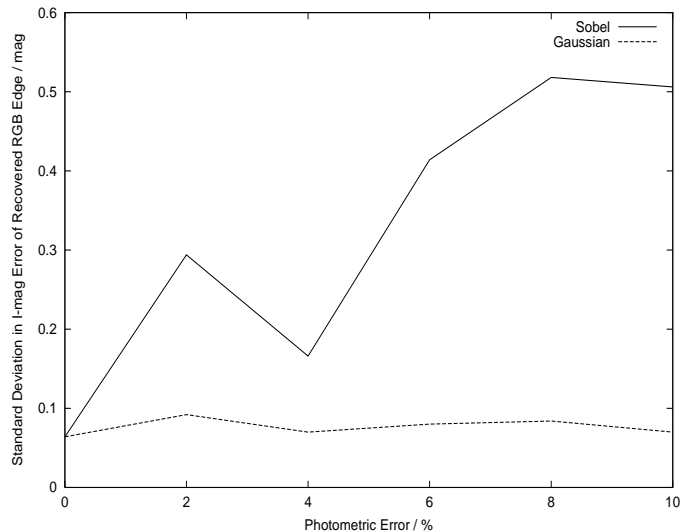


**Figure 10.** Testing the new Gaussian method for estimating the TRGB magnitude in simulated stellar populations. Varying photometric errors have been used. Population details remain the same as that in figure 7. Clearly the Gaussian method remains superior at all levels of photometric error.

metric error levels. It is hardly affected at all by the introduction of severe photometric errors, as one would expect.

### 3.2 Conclusions

We therefore suggest a new method for estimating TRGB distances in average- to poorly-populated CMDs by fitting the above proposed Gaussian cutoff (formula 1) to the TRGB luminosity function and solving for a fixed point on

the curve, such as the zero of the 2nd differential at  $I = c + b$ . We propose that this method is robust to numerical errors, and allows an accurate determination of the TRGB distance especially for populations with a poorly-defined RGB tip.

For larger datasets, that is if there are at least 1000 stars within one magnitude of the TRGB, the standard edge-detection method seems more robust, though we instead suggest adoption of the technique outlined by Cioni et al. (2000) using the second derivative of the luminosity function. They report that this method works more reliably than the traditional Sobel filter method, though obviously it will still suffer from the above described numerical errors with smaller datasets.

We now present an application of the current work to real astronomical datasets in order to demonstrate its effectiveness and accuracy. We present two different datasets in order to test the robustness of our code in different situations.

#### 4 MILKY WAY GLOBULAR CLUSTERS

We obtained a set of 20 CMDs from the publically available archive of Rosenberg et al. (2000) and tested our code on all of them. One of the most important effects we noticed was the inability for our code to fit very metal-poor populations, due to isochrone limits. This permits us only to obtain an upper limit on the true metallicity.

The reason why we obtain only a limit on the metallicity is simply because we don't have any isochrones beneath  $Z = 0.0004$ . We run into problems with the weighting profiles as soon as we get near this limit, as the following diagrams show (see Fig. 11), due to the fact that all the weighting for metallicities lower than  $Z = 0.0004$  is added to the  $Z = 0.0004$  isochrone, as this is the nearest to the correct value. It is impossible to obtain a true value for metallicities lower than about  $Z = 0.0006$  because of this shortfall. The exact value depends, of course, on the metallicity interpolation granularity in the isochrone set. As a limit, after some testing, we determined that the lowest metallicity peak we could accurately detect was approximately that of the 4th most metal-poor isochrone.

Of course, in reality values of  $Z < 0$  are not possible, so there is actually a fundamental limit to which we can obtain metallicity peaks by this method, regardless of isochrone spread. At these levels we are running into clear problems with our initial assumption that most star formation events produce stars with a roughly Gaussian metallicity distribution.

Of all those datasets we managed to fit, after reddening correction and the inclusion of the best literature values for the age and distance modulus to each cluster, all but 3 were within 0.3dex of the Harris (1996) value for the central metallicity. Some of the variation in our results from the accepted values may well be due to the inaccuracies in converting metallicity abundances into  $[Fe/H]$ . The three badly-fitting clusters were NGC 5927, NGC 104 (47Tuc) and NGC 6205.

We also calculated the errors between the retrieved metallicity estimates given the two assumed ages 10 Gyr and 13 Gyr. We found that the estimated absolute value of

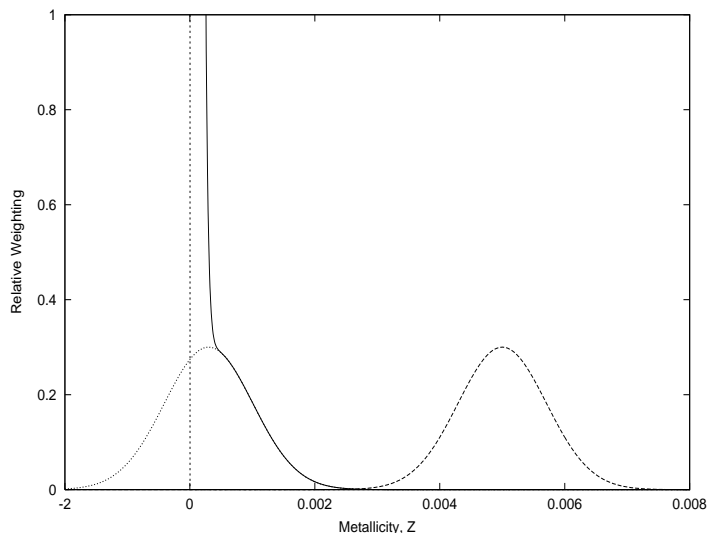


**Figure 11.** The minimum metallicity we can accurately detect is approximately  $Z = 0.0006$ , due to the limits of the weighting scheme we employ. At higher metallicity (rightmost peak) we detect the peak accurately. When the metallicity gets very low (leftmost peak) then every metallicity value lower than our lowest-metallicity isochrone is added together into the lowest-metallicity weighting value. The dotted line shows the true shape, and the solid line shows the recovered profile. Because of this effect, it becomes impossible to detect peaks accurately if the true mean falls within the first three or four isochrone metallicity values.

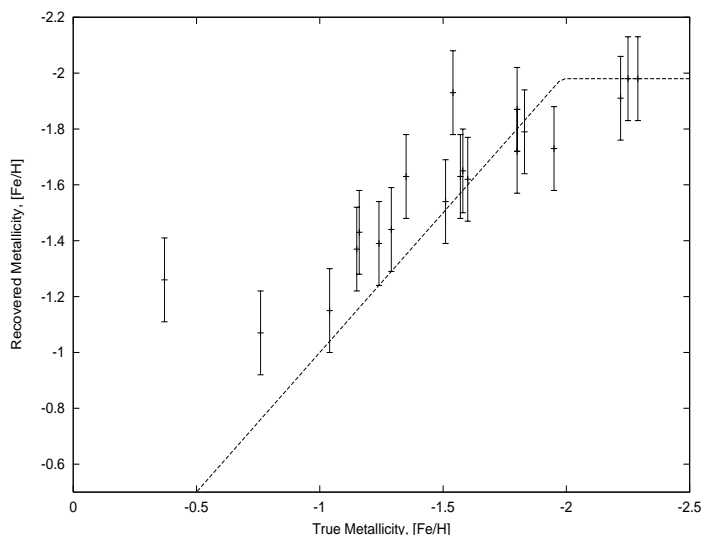


**Figure 12.** Comparing our metallicity fits to Milky Way Globular Clusters with the literature values of Harris (1996). Error bars are 0.15 dex, calculated as the sum of the estimated uncertainties due to distance and age examined above.

the discrepancy was  $[Fe/H] \simeq 0.085dex \pm 0.020dex$  for our sample.

## 5 URSA MINOR DWARF SPHEROIDAL GALAXY

The Ursa Minor dwarf spheroidal galaxy is a satellite galaxy to the Milky Way, located at approximately 66 kpc from the sun (Mateo, 1998, henceforth M98). It is known to be a relatively simple stellar population, containing mainly old stars, and possessing a narrow abundance distribution. M98 suggests a single, large star formation between 10-14 Gyr ago, which produced all the stars within the galaxy. Ursa Minor has since remained untouched by outside influence, except for the inevitable tidal disruption caused by the Milky Way's gravitational potential.

As such, UMi is an interesting and instructive target with which to test our code, knowing that we don't expect a purely coeval stellar population, but that the contamination from young stars is low to negligible. It provides a suitable branch from the simplistic, coeval globular clusters to the more complicated, spatially and chronologically extended dwarf members of the local group.

### 5.1 The data

We took our data from the photometry of Kleyna et al. (1998) who present a Johnson-Cousins  $V, I$  mosaic survey of the entire central region of the UMi dwarf spheroidal to  $V \simeq 22$ , taken using the F. L. Whipple Observatory (FLWO) 1.2 m telescope. These data consist of 27 fields, imaged twice in each of  $V$  and  $I$  for 300s per exposure. Full details of the preliminary data reduction can be found in Kleyna et al. (1998).

We obtained the full photometry dataset for all objects detected in the 27 fields, together with an estimate of the stellarity of each source as calculated by the SEXtractor programme (Bertin & Arnouts, 1996). Non-stellar objects were removed by imposing a selection criterion of *stellarity*  $> 0.7$ . Further cuts were made in both absolute  $I$  magnitude and  $V - I$  colour in order to remove as large a fraction of contaminant foreground stars as possible. Stars with  $I < 19.0$  were removed, together with all stars outside the range  $0.75 < V - I < 1.6$ . This left the RGB stars, together with a significant amount of contaminants surrounding them. This would therefore prove an excellent test of the ability of our *FITCOEVAL* programme to ignore contaminants and pick out principal stellar components from amongst noise.

Fig. 13 shows the complete CMD for stellar objects in UMi, together with the imposed cuts which we employed to select only the RGB population.

After obtaining the RGB population, we then added a reddening correction using the literature value of  $E(B - V) = 0.03 \pm 0.02 \text{ mag}$ . Following this, we ran our code on these data using the two spanning isochrones of 10 Gyr and 13 Gyr. Each of these were taken from a *finex* set, interpolated to 200 metallicity subdivisions between  $Z = 0.0004$  and  $Z = 0.01$ . The assumed distance was  $(m - M)_V = 19.11$ , from M98. The optimum fits calculated are shown in Fig. 14.

The maximum values for each of these fits were  $Z = 0.00069$  for the 10 Gyr isochrone fit, and  $Z = 0.00064$  for the 13 Gyr isochrone fit. These correspond to iron abundances of  $[Fe/H] \simeq -1.79$  and  $-1.82$  respectively. Standard values for

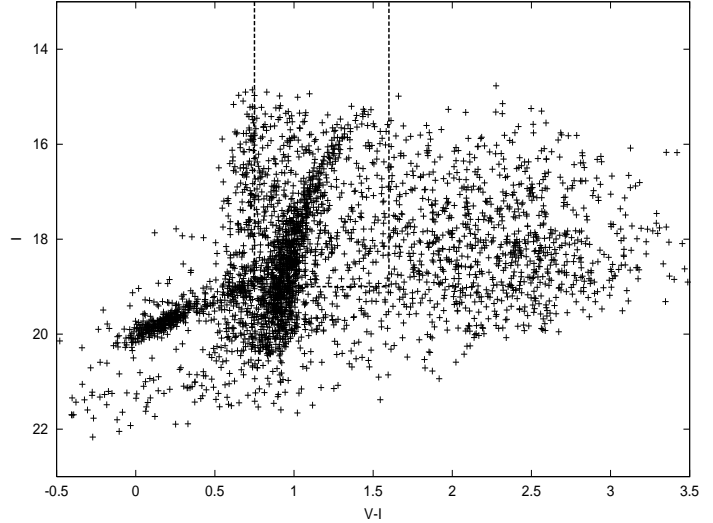


**Figure 13.** A CMD for the 4,370 stellar objects selected from the original UMi photometry. The solid lines show the cuts in both  $I$  magnitude and  $V - I$  colour imposed in order to select only the RGB population with as little contamination as possible. 1021 stars passed the selection criteria.

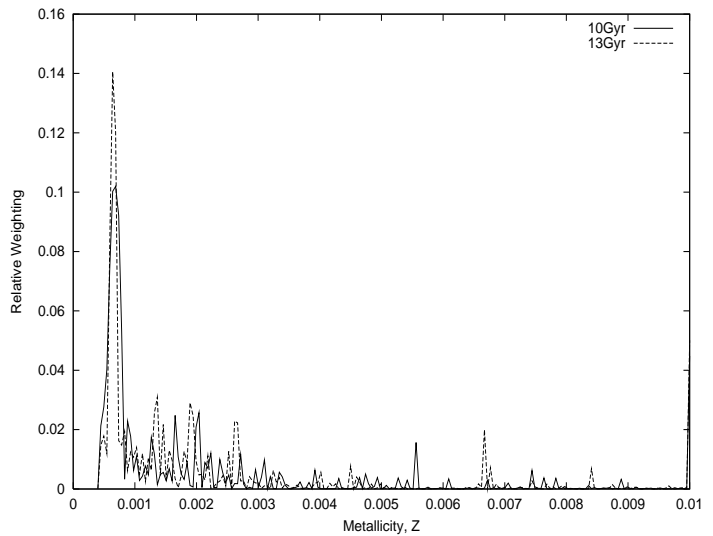


**Figure 14.** Full reduction of the UMi data using an assumed distance of  $(m - M)_V = 19.11$ , and isochrones of 10 Gyr and 13 Gyr.

UMi place the iron abundance at roughly  $[Fe/H] \simeq -2.1$ . (See, for example, M98).

As calculated earlier, we can estimate an error on this value of approximately  $0.15 \text{ dex}$  from the uncertainties in distance and age. The uncertainty in the reddening is small ( $0.02 \text{ mag}$ ). Using the lower value of  $E(B - V) = 0.01 \text{ mag}$  alters the derived  $[Fe/H]$  value by less than  $0.01 \text{ dex}$  in  $[Fe/H]$ . Choosing a higher value of  $E(B - V) = 0.05$  results in a much poorer fit with a significantly lower final likelihood. It provides a pair of maxima in the resultant metallicity distribution around  $Z = 0.00064$  and  $Z = 0.00088$ , corresponding to  $[Fe/H] = -1.82$  and  $-1.68$  respectively.



## 6 CONCLUSION

Our code appears reasonably robust to sensible photometric errors, and is able to recover the central metallicity of a globular cluster stellar population in most (75% of) cases. Resolution is restricted to a lowest metallicity of  $[Fe/H] \simeq -1.9$  due to numerical considerations. At lower metallicity, resolution in  $[Fe/H]$  is reduced due to the logarithmic nature of the iron abundance scale.

Age, reddening and distance errors should not be a great problem unless they vary by a significant value, where ‘significant’ here means 2–3 Gyr in age, 0.1 mag in  $V$ -extinction or 0.2 mag in distance modulus.

C.M.F. would like to extend his thanks to Jan Kleyna for help in the preparation of the code required for this project, and also to Lynette Dray, Brian Chaboyer and Richard de Grijs for interesting discussions on these topics.

## REFERENCES

- Bellazzini M., Ferraro F.R., Pancino E., 2001, *ApJ*, 556, 635  
 Bergbusch P.A., Vandenberg D.A., 2001, *ApJ* 556, 322  
 Bertelli G., Betto R., Chiosi C., Bressan A., Nasi E., 1990, *A&AS* 85, 845  
 Bertin E., Arnouts S., 1996, *A&AS*, 117, 393  
 Cioni M.-R.L., van der Marel R.P., Loup C., Habing H.J., 2000, *A&A*, 359, 601  
 Da Costa G.S., Armandroff T.E., 1990, *AJ*, 100, 162  
 Ferrarese L., et al. 1996, *ApJ*, 464, 568  
 Frayn C.M., Gilmore G.F., 2002, *MNRAS*, In Press  
 Girardi L., Bressan A., Bertelli G., Chiosi C., 2000, *A&AS*, 141, 371  
 Harris J., Zaritsky D., 2001, *ApJS*, 136, 25  
 Harris W.E., 1996, *AJ* 112, 1487  
 Kleyna J.T., Geller M.J., Kenyon S.J., Kurtz M.J., Thorstensen J.R., 1998, *AJ*, 115, 2359  
 Maeder A., Meynet G., 1991, *A&ASS*, 89, 451  
 Mateo M.L., 1998, *ARA&A*, 36, 435  
 Mathis J.S., 1990, *AnnRev.*, 28, 37  
 Rogers F.J., Iglesias C.A., 1996, *AAS*, 188, 5804  
 Rosenberg A., Aparicio A., Saviane I., Piotto G., 2000, *A&AS*, 144, 5  
 Sakai S., Madore B.F., Freedman W.L., 1996, *ApJ*, 461, 713  
 Salaris M., Cassisi S., 1997, *MNRAS*, 289, 406  
 Salaris M., Chieffi A., Straniero O., 1993, *ApJ*, 414, 580  
 Salaris M., Cassisi S., Weiss A., 2002, *PASP*, 114, 375  
 Yi S., Demarque P., Kim Y.-C., Lee Y.-W., Ree C.H., Lejeune T., Barnes S., 2001, *ApJS*, 136, 417  
 Yildiz M., Kiziloglu N., 1997, *A&A*, 326, 187

## 7 APPENDIX : DIFFICULTIES WITH ISOCHRONES

We briefly summarise some possible sources of systematic error in an adopted set of isochrones.

In using the process of isochrone fitting, it is important first to investigate the uncertainties caused by the isochrones themselves. As theoretical models, they have a considerable number of parameters whose values can be changed, often causing significant differences between different isochrone models.

A slight variation in the model definition at some rapid evolutionary stages can give a drastically different isochrone. See, for example, the early work done on convective overshooting by Bertelli et al. (1990). The isochrone set that we have mainly adopted for use in this study is that by Girardi et al. (2000).

In general, the HB is very poorly understood in the theoretical models, with little consensus on the true nature of the second parameter problem, and few groups agreeing well on the predicted shape. The horizontal branch occupies a relatively compact area of the CMD, where small errors in photometry can give very large errors in derived metallicity and hence errors in either the models or the photometry in this regime. None of the isochrone sets we have tested could accurately reproduce very blue HBs, such as that exhibited by the galactic globular cluster NGC 288, amongst others.

Furthermore, if we continue the photometry even deeper then we approach the main-sequence turn-off, where problems are caused by blue straggler stars which are obviously not fitted at all well by any existing isochrone models, being creations of stellar dynamics rather than isolated stellar evolution. Binary stars can also cause problems, with theoretical isochrones only representing single stellar systems.

### 7.1 Problems modelling the RGB

The red-giant branch poses many unsolved problems for theoretical modellers, and is consequently fairly inaccurately represented in most theoretical isochrones. One such important problem is that of mass-loss. RGB stars are highly expanded with only tenuously retained outer layers. Stars at this stage in their evolution tend to lose a substantial fraction of their mass through stellar winds.

Fortunately for the purposes of this study, mass loss on the RGB is only a very minor effect for low-mass stars. Provided it is treated sensibly, it can almost be neglected. Certainly for stars less than one solar mass, this will not affect the isochrone models to any significant degree.

In addition, stellar atmospheres are not understood particularly well on the RGB, leading to slightly larger colour-errors in these sections of the models. This affects all mass-ranges. If one uses Kurucz model atmospheres then the deviation from accuracy towards the faint end of the RGB can be significant. There is not a great deal that can be done to rectify this problem, and the safest assumption seems to be to reduce the weighting for stars near the tip of the RGB by introducing slightly larger underlying intrinsic errors in this regime.

Derived values of the TRGB level vary by around 0.2 magnitudes between individual theoretical studies. This uncertainty is primarily caused by uncertainties in the RGB

modelling schemes used, and illustrates why isochrone fitting must therefore remain an unreliable method for obtaining absolute, quantitative values for the internal parameters of stellar populations to any useful degree of confidence.

Finally, as mentioned in section 7.2.2 below, mixing length theory and the choice of surface boundary conditions can cause substantial variation of the RGB model predictions. The reader is referred to sections 5.6 and 5.7 of the review by Salaris et al. (2002) which covers these topics in considerable detail.

## 7.2 Tuneable parameters

Inherent in the theoretical models used to generate model isochrones, there are a number of poorly-understood parameters whose values may be tuned in order to generate the required results. Often these parameters are altered so that the isochrone fits a certain realistic CMD, but this is not always the case.

### 7.2.1 Equation of state and opacities

Adopted stellar opacity laws are continually being updated. Corrections from modern opacity calculations are rather smaller than could be expected a generation ago, but they are still considerable under some circumstances. Several studies have been performed on the effects of varying the opacity and equation of state used in calculations, see for example, Yildiz & Kiziloglu (1997).

Rogers & Iglesias (1996) have extended the standard OPAL opacity laws down to lower stellar masses beneath  $0.8M_{\odot}$ , therefore allowing more accurate modelling of RGB stars in truly old, metal poor stellar populations. The lifespan of an  $0.8M_{\odot}$  star is approximately one Hubble time however, so these low-mass stars will not yet have reached the RGB stage in most cases.

### 7.2.2 Mixing length theory & convective overshooting

Mixing length theory comes from models of convective stars, and consequently applies strongly to younger, more massive stars with convective cores. However, it is also used in predicting the behaviour of the convective envelopes of low-mass stars, to determine the temperature gradient in superadiabatic regions. Hence the mixing length parameter determines the effective temperature of stars with convective envelopes, such as the RGB stars in which we are primarily interested.

For more massive stars, generally those above  $1.6M_{\odot}$ , the free parameter of the overshooting distance also becomes important. This was treated in considerable detail by Maeder & Meynet (1991). They claimed that including convective overshooting in their models could revise estimated ages of Red Turnoff stars upwards by a factor of between 1.5 and 2.7. Estimating the ages from the Blue Turnoff gave errors in age determinations of factors between 1.6 and 2.2.

All isochrone models now include these parameters, but the actual extent to which the convective overshooting model is applied, and the value for the mixing length are still very much open to debate, and can actually cause a substantial difference in the model colours obtained.

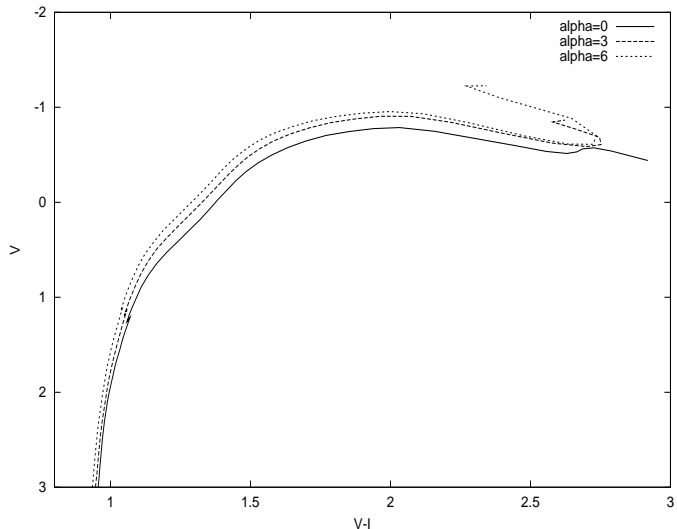


**Figure 15.** Here we have plotted isochrones for 10 Gyr with metallicity of one half solar abundance, varying the alpha element ratios to  $[\alpha/Fe] = 0.0, 0.3, 0.6$ . The difference is not enormous, but could cause a shift in the assumed metallicity for RGB populations.

### 7.2.3 $\alpha$ -element ratios

Salaris, Chieffi & Straniero (1993) examined in detail the degree to which alpha-enhanced isochrone models alter the fits obtained to the galactic globular cluster system and concluded that evolutionary properties of stellar models depend significantly on the adopted abundances of all the  $\alpha$ -elements. They also discovered that adopted opacity laws can have a substantial effect on the shape of an isochrone, especially at low metallicity and low temperature.

Recently, the Yale-Yonsei group have released a set of theoretical isochrone tracks with varying alpha-element ratios (Yi et al., 2001). Figure 15 shows the differences between alpha-element ratios of  $[\alpha/Fe] = 0, 0.3, 0.6$ . Interpolation code kindly donated by Sukyoung Yi.

Varying alpha enhancement ratios gives us yet another degeneracy. In Fig. 16 it is clear that the variation between alpha element enhancement of  $[\alpha/Fe] = 0.0$  and  $0.3$  at an age of 10 Gyr and metallicity of half-solar, is approximately the same as that caused by a metallicity increase of 20%. This gives us another contribution to the error on our metallicity measurements.

The systematic effects of incorrectly modelled alpha element abundances can only have a small differential effect. For example, in modelling galactic globular clusters, all clusters may exhibit similar alpha-element ratios, and thus any error in assuming an incorrect alpha-element ratio for the isochrones will result in a constant shift for all clusters, retaining exactly the correct ordering if not the precise metallicity values.

### 7.2.4 Parameter fine-tuning

With so many parameters, it is usually possible to alter stellar models in such a way so as to fit an observed population with a reasonable age and metallicity spread. Many groups, for example Bergbusch & VandenBerg (2001) do ex-

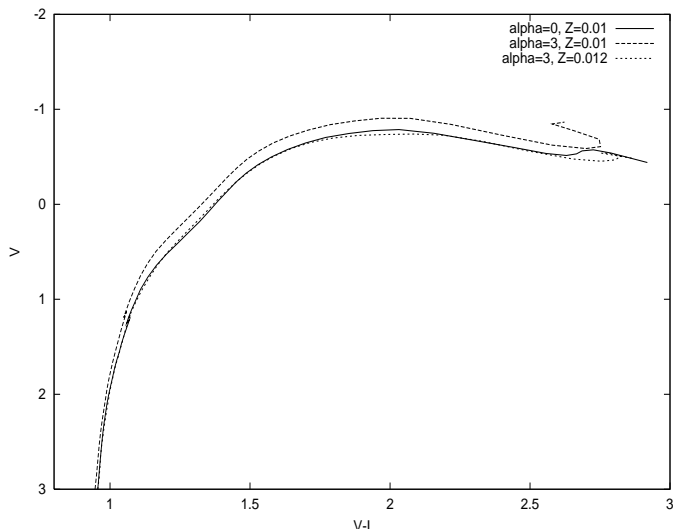


**Figure 16.** Here we have plotted isochrones for 10 Gyr with metallicity of one half solar abundance, varying the alpha element ratios to  $[\alpha/Fe] = 0.0, 0.3$ . In addition, we have overplotted an isochrone for  $[\alpha/Fe] = 0.3$  and metallicity 20% higher. The effects of varying metallicity and  $[\alpha/Fe]$  are very similar.

actly this, tuning their isochrones so that they fit a set of template populations, as well as standard data for the sun. In this case, comparisons are made with galactic globular clusters M3 and M92, and the assumption is that these populations are representative.

In some sense what we are doing here is using the answer as a starting block for our models, and then we should not be too surprised when our models give us back the answer upon which we based them. However, once one moves to different clusters, and indeed other stellar populations, such as Population II halo stars, the benefit of this method becomes apparent. Of course, we are assuming that there is some underlying law, or set of laws, which unify all stellar populations given a set of observable parameters. Observations show us that this might not necessarily be the case. It is only an assumption that models tuned to fit globular clusters should be preferentially more accurate in analysing stellar haloes.

Even after fitting their models to a wide range of MWG globular clusters, Bergbusch & Vandenberg still found that their models failed to predict the observed luminosities of the red giant bump by  $\simeq 0.25\text{mag}$ . No matter how accurately model parameters are optimised, there is always the danger that we have neglected some fundamental physics which complicates the situation.

### 7.3 Non-linear isochrone interpolation

When interpolating between isochrones, we are forced to make some simplifying assumptions. One such assumption is that a linear interpolation is sufficiently accurate for our needs. That is, we assume that e.g. between two isochrones of metallicity  $Z = 0.01$  and  $Z = 0.011$  there might be another 9 isochrones all spaced by 0.0001 in metallicity,  $Z$ . However, the assumption that these interpolated isochrones

should lie exactly evenly spaced in colour-luminosity space is one that might not be valid.

However, when interpolating new isochrones we already have a great deal of difficulty pairing off the four isochrones spanning our desired age/metallicity values in both these variables. To improve on the linear interpolation assumption would require spline-fitting from previous isochrones, which would then need to be paired off with the target isochrones in a similar way. This method then rapidly becomes unfeasible.

The best guess we can make is that the isochrones do not behave pathologically and that, in the absence of other information, isochrones linearly spaced in metallicity should be linearly spaced in the colour-luminosity variables that we are calculating.

Further interpolation problems lie with the isochrone masses. Isochrones are parametrized as a series of points approximating a parametric curve. However, assuming straight-line sections joining these points can introduce errors in the assumed masses, and therefore the occupation probabilities for those points. Harris & Zaritsky (2001) investigated this problem, and discovered two important things;

- The error is never more than a few hundredths of a solar mass, and is therefore fairly insignificant in terms of IMF variability.
- The error is negligible for stars brighter than the MSTO, i.e. all the stars in which we are interested.

Bergbusch & Vandenberg (2001) introduce the concept of an Akima spline for interpolation accurate colours around the MSTO. Again, these effects are small, being of the order  $\Delta T_{eff} \simeq 0.001 T_{eff}$ , and are confined to low-luminosity stars.

We therefore neglect these effects entirely.

### 7.4 Conclusions

Isochrone fitting clearly has its limitations, but once these are accepted and dealt with as effectively as possible, it becomes a powerful method for analysing stellar populations. However, one must be aware of the inherent problems and understand that any results obtained are only useful in a relative sense; the absolute age and metallicity values are likely to be highly unreliable in some cases.

Most importantly, the uncertainty in isochrones is most apparent in young, high mass models where more extreme and poorly understood physics is operating. Not surprisingly, models of solar-mass stars are good. For the studies which are considered in this work, very few stars are above one solar mass. Most populations are of 10 Gyr or older, at which age the oldest star on the RGB will have an initial mass of only fractionally above one solar mass for a solar metal abundance (from Girardi et al. isochrones). The worst of these problems can therefore be safely neglected.